Dominant Effect of Polariton-Polariton Interactions on the Coherence of the Microcavity Optical Parametric Oscillator

D. N. Krizhanovskii,[1] D. Sanvitto,[1] A. P. D. Love,[1] M. S. Skolnick,[1] D. M. Whittaker,[1] and J. S. Roberts[2]
[1]*Department of Physics and Astronomy, University of Sheffield, Sheffield S3 7RH, United Kingdom*
[2]*Department of Electronic and Electrical Engineering, University of Sheffield, Sheffield S1 3JD, United Kingdom*
(Received 18 January 2006; published 31 August 2006)

The importance of interaction effects in determining the temporal coherence of spectrally and spatially isolated single modes of the microcavity optical parametric oscillator (OPO) is demonstrated. As a function of macroscopic occupancy, the coherence time (τ_c) first increases linearly and then exhibits saturation behavior, reaching maximum values of up to 500 ps. Good agreement is found with a model including fluctuations in polariton number and polariton-polariton interactions between the OPO states. τ_c is a property of the coupled OPO system, a result confirmed by the finding of equal coherence times for signal and idler, even though the idler is subject to strong additional scattering.

DOI: 10.1103/PhysRevLett.97.097402 PACS numbers: 78.67.−n, 42.25.Kb, 42.55.Sa, 71.36.+c

Temporal and spatial coherence are fundamental properties which characterize systems that undergo a transition into a high density, macroscopically occupied state. Such macroscopic occupations can be achieved in semiconductor microcavities (MCs) [1], where optical parametric oscillator (OPO) behavior is observed under resonant excitation of the lower polariton (LP) branch [2]. The thresholdlike behavior of the OPO, where signal and idler states [see Fig. 1(a)] are formed in a dynamical equilibrium between the driving pump field and the cavity losses, has similarities to that seen in a photon laser. However, the exciton content in the polariton gives rise to interparticle interactions, which we show here influence strongly the properties of the coherent emission and, hence, of the high density phase.

Up to the present, most studies of the microcavity OPO have investigated basic properties such as angular distribution [2], polarization [3], power [2,4], and temperature [5] dependence. Quantum phenomena such as squeezing [6] and complementarity of idler polaritons [7] were also reported. The theoretical work of Ref. [8] predicts the formation of macroscopic spatial coherence of the OPO signal driven by a laterally uniform laser field. Experimental evidence for coherence of degenerate parametric scattering was shown in quantum noise measurements [9].

We show, using a single frequency laser for excitation, that the signal consists of a number of narrow, spatially and spectrally distinct modes with a localization size of $\sim 10\ \mu$m. Using spatial and spectral filtering to isolate individual modes, we study the coherence of the OPO emission. The coherence times exhibit saturation behavior with increasing state occupancy and achieve maximum values of ~ 500 ps. The effect is explained by polariton-polariton interactions between macroscopically occupied signal, idler, and pump states. The resultant blueshift of the OPO states, together with fluctuations of the polariton population, leads to a reduction of the coherence time with occupancy. In the coupled OPO system, energy and phase conservation for the scattered particles require energy and phase fluctuations of the signal and idler to be anticorrelated, explaining the finding that the coherence times of the signal and idler are very similar over the whole range of excitation powers.

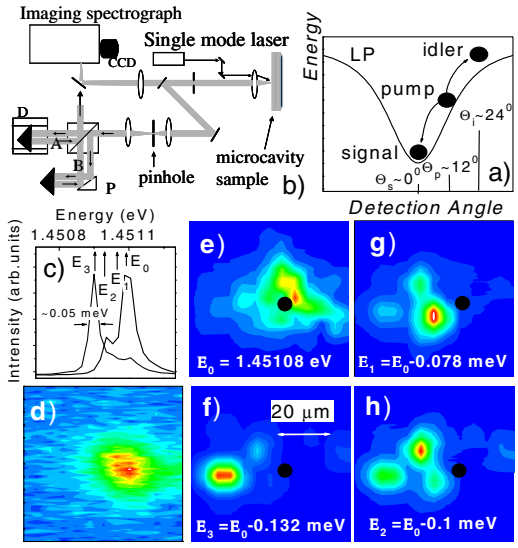

FIG. 1 (color online). (a) Polariton dispersion curve showing scattering into signal and idler states. (b) Schematic diagram of the experimental setup. The positions of mirrors P and D in the Mach-Zehnder interferometer determines the course delay time and the phase shift between beams A and B, respectively. (c) Spectra corresponding to stimulated polariton emission from the bottom of the LP branch at excitation power $P = 31$ mW, recorded from two spatially separated slices of $5 \times 40\ \mu$m dimension across the excitation spot. (d)–(h) Spatial images of the polariton emission for (d) $P = 1.5$ mW and (e)–(h) $P = 31$ mW. The detection energies E_0–E_3 for images (e)–(h) are given on the images and are marked on the spectra. The center of the pump is indicated by the black solid circle in (e)–(h).

The structure of the MC studied is very similar to that of Ref. [2]. Several positions on the sample were investigated with Rabi splitting $\Omega \sim 6$ meV and near zero detuning between exciton and cavity modes. The beam from a single frequency diode laser (FWHM ~ 10 MHz) was focused to ~ 40 μm on the sample at an angle of incidence of $\Theta_p = \sim 12°–15°$ to achieve resonant excitation of the LP branch. Spatially and spectrally resolved images of the LP emission (collected in a solid angle $0 \pm 5°$) were recorded [see Fig. 1(b)]. First order correlation functions were measured using a Mach-Zehnder interferometer.

Figure 1(c) shows spectra from the bottom of the LP branch (the signal emission at $\Theta_S = \sim 0°$) at excitation powers $P = 31$ mW well above the threshold ($P_{\text{th}} \sim 3$ mW) for stimulated polariton-polariton scattering. The spectra are recorded from two spatially separated sections of $\sim 5 \times 40$ μm dimension across the 40 μm excitation spot. The emission consists of a number of narrow features with an energy separation and linewidth of 0.05–0.06 meV (FWHM, resolution limited). As seen in Fig. 1(c), different peaks dominate depending on the detection area across the spot.

Spatially resolved images (5 μm resolution) of the signal are presented in Figs. 1(d)–1(h). Each individual image in Figs. 1(e)–1(h) is recorded at a specific emission energy [E_0–E_3 for Figs. 1(e)–1(h) on the spectra of Fig. 1(c)]. Below threshold in Fig. 1(d) at a power $P = 1.5$ mW, the LP emission has a near-Gaussian distribution, determined by the excitation beam. By contrast, at $P = 31$ mW above threshold [Figs. 1(e)–1(h)] the signal consists of a number of spatially separated modes [spectrally resolved in Fig. 1(c)] with a localization size of ~ 10 μm and with emission at different energies. The energy of the mode decreases with an increase of the localization distance from the excitation spot [the solid black circle in Figs. 1(e)–1(h)]. The use of the single mode pump laser results in narrowing of the signal spectra and allows the spectral resolution of the mode structure. By contrast, the spectral structure was not resolved in previous studies [2,3,5] where a multimode Ti:sapphire laser with a linewidth of ~ 0.05 meV was used.

Spatial resolution allows us to isolate one mode and to study its evolution with power. Figure 2(a) shows normalized signal spectra versus P for a ~ 5 μm region within the images of Figs. 1(d)–1(h). Below threshold, the LP emission is broad (FWHM ~ 0.25 meV) corresponding to incoherent population of states close to $k = 0$. Above threshold ($P_{\text{th}} \sim 3$ mW), standard microcavity OPO behavior is observed [2]: The emission transforms into a single narrow peak, which grows superlinearly [Fig. 2(b)] and exhibits the characteristic blueshift in the range from 5 to ~ 30 mW [10]. The blueshift arises from the repulsive polariton-polariton interactions [11,12] between signal, pump, and idler states.

A full discussion of the origin of the spatial structure is given elsewhere [13] within the quasiclassical formalism of the microcavity OPO; we restrict ourselves here to a summary of the points needed for the present discussion. Two main mechanisms give rise to the spatial nonuniformity of the signal. First, the pump field has a Gaussian profile, and so the blueshift of the signal is maximum at the center of the spot and decreases towards the edge. Second, there are fluctuations in the photonic potential of ~ 0.1 meV possibly due to misfit dislocations in the Bragg mirrors [14], which contribute to a spatial variation of the signal energy. These effects inhibit the formation of macroscopic spatial coherence of the signal [8], which breaks up into localized modes with different energies [Figs. 1(e)–1(h)].

Having achieved spectral and spatial resolution of individual signal modes, we are able to investigate the coherence properties of the OPO. Since the linewidth $\Delta\nu$ (or coherence time $\tau_{\text{coh}} \sim 1/\Delta\nu$) of the spatially resolved signal modes was below the resolution of typical grating spectrometers, we employed a Mach-Zehnder interferometer to study the coherence properties. As seen in Fig. 1(b), the spatially selected signal was directed through the interferometer and the intensity at the output of the spectrometer recorded as a function of phase shift for different course delay times τ_d. Typical interference patterns for the signal and idler (open and solid squares), at a power of 23 mW well above threshold, are shown in Fig. 3(a) at $\tau_d = 180$ ps. The first order correlation function $g^1(\tau_d)$ of the signal is given by the visibility $g^1(\tau_d) = \langle E^*(t)E(t+\tau_d)\rangle / \langle E^*(t)E(t)\rangle = (I_{\max} - I_{\min})/(I_{\max} + I_{\min})$ of the interference fringes versus delay time (E is the electric field, and $I_{\max,\min}$ are maximum and minimum intensities of the

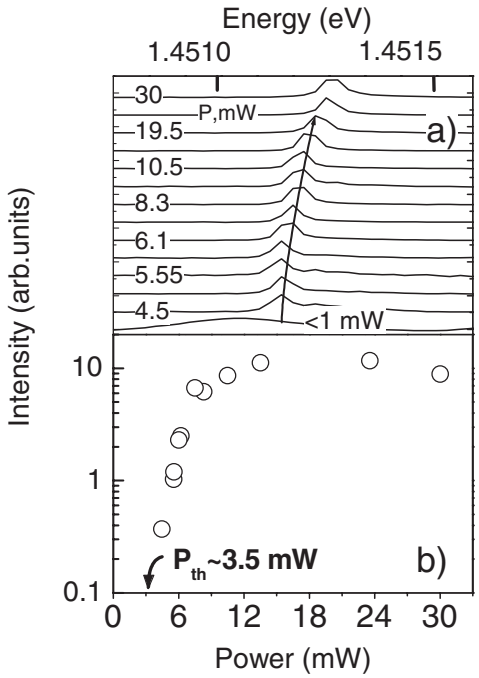

FIG. 2. Signal spectra from the spatially filtered area of radius ~ 5 μm versus excitation power P. (b) Intensity of the signal emission versus pump power P.

interference fringes). Figure 3(b) shows a typical dependence of $g^1(\tau_d)$ for the signal above threshold, decaying exponentially within a coherence time $\tau_{\rm coh}$ of ~230 ps. As a control, the visibility of the fringes for the laser was measured and found to be 0.95 at $\tau_d \sim 120$ ps [Fig. 3(a)], indicating the coherence time of the pump to be more than 1 order of magnitude longer than that of the signal.

To provide information on the factors determining the OPO coherence, $\tau_{\rm coh}$ was studied as a function of excitation power [15] for both the signal and idler at detection angles $\Theta_s \sim 0$ and $\Theta_i \sim 24°$ [Fig. 1(a)], respectively. From the ratio of the signal to idler intensities, the signal population N_s is deduced to be a factor of 5–10 larger than that of the idler N_i. The idler depletion mainly arises due to ''idler-idler'' and ''idler-pump'' scattering towards high k exciton states [12].

Surprisingly, despite the extra scattering channel out of the idler state, both the signal and idler have very similar coherence times, as seen from comparison of their interference patterns which have very similar visibilities [Fig. 3(a), the solid and open squares]. Moreover, as shown in Fig. 3(c), very similar coherence times for the signal and idler are observed over the whole range of pump powers [16]. Coherence times ($\tau_{\rm coh}$) of ~100 ps are observed at powers just above threshold. As a function of signal intensity ($I \propto N_s$), a linear increase is then seen, followed by saturation behavior at values of ~500 ps.

In a noninteracting stimulated system such as a laser [17,18], the coherence time is proportional to the ratio of the number of stimulated to noise photons, due to spontaneous emission into the lasing mode. In the OPO, spontaneous scattering occurs within a time $\tau_{\rm sp} \sim 1/\sqrt{\gamma_s \gamma_i} \sim 5$ ps, determined by the polariton losses, where γ_s and γ_i are polariton linewidths below threshold. Therefore, making the analogy with the laser and assuming the limitation of the OPO coherence only by spontaneous scattering, the coherence time of the signal and idler is expected to vary linearly with polariton population $(N_s + N_i) \approx N_s$ ($N_s \gg N_i$) and is given by $\tau_{\rm coh} = \langle N_s \rangle \tau_{\rm sp}$. The predicted linear behavior is in contrast to the saturation in the variation of $\tau_{\rm coh}$ with N_s found in Fig. 3(c). We note that, despite the strong depletion of the idler population, the coherence times of signal and idler are expected to be the same within this picture, since an equal polariton flux into these states due to polariton-polariton scattering implies the same fractional contribution of spontaneous noise polaritons for the signal and idler.

The observed variation of the temporal coherence with N_s finds a natural explanation if polariton-polariton interactions are included [19]: The interactions affect not only the spatial patterning of the OPO as discussed above, and hence spatial coherence, but also the temporal coherence. The repulsive interaction leads to the blueshift in energy mentioned above, determined by the total polariton population in the system [11,12]. Following Ref. [12], for a fixed energy of the pump, the energy shift of the signal with

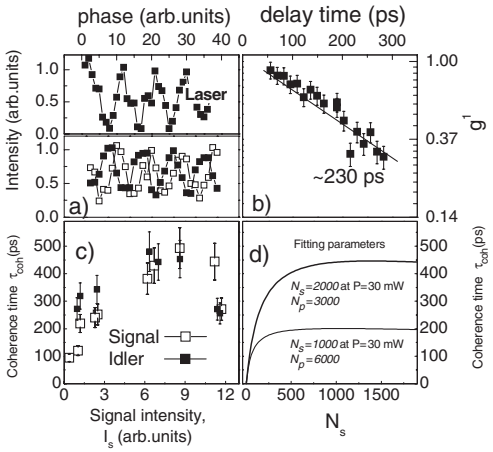

FIG. 3. (a) Interference fringes as a function of phase shift between the beams in the two arms of the Mach-Zehnder interferometer for the pump laser, the signal (open squares) and the idler (solid squares). (b) A typical variation of the g^1 function versus delay time for an isolated signal mode above threshold. (c) Coherence times $\tau_{\rm coh}$ of the individual signal (open squares) and corresponding idler (solid squares) modes versus signal intensity I_s. (d) Calculation of the signal coherence time versus signal polariton population N_s.

respect to the energy of the lower polariton branch below threshold, determined by the polariton-polariton interactions between pump, signal, and idler states, is given by

$$\Delta E_s \sim \chi^3 \Big[\frac{|X_s|^4 \gamma_i}{(\gamma_i + \gamma_s)} \Big(N_s - N_i \frac{\gamma_s |X_i|^4}{\gamma_i |X_s|^4} \Big) + \frac{2|X_p|^2}{(\gamma_i + \gamma_s)} \times (\gamma_i |X_s|^2 - \gamma_s |X_i|^2) N_p \Big]. \quad (1)$$

$N_{s,p,i}$ is the mean number of polaritons in the signal, pump, and idler, respectively, $\gamma_s \sim 0.3$ meV, $\gamma_i \sim 1$ meV are the polariton linewidths below threshold, $|X_s|^2 \sim 0.5$, $|X_p|^2 \sim 0.7$, and $|X_i|^2 \sim 0.95$ are the excitonic contents of the signal, pump, and idler states, respectively, and χ^3 is proportional to the third order nonlinearity coefficient which determines the strengths of the scattering processes. The energy of the idler is given by energy conservation by $E_i = 2E_p - E_s$.

In macroscopically occupied states, there are always fluctuations in the number of particles. For coherent states, the minimum amplitude of the fluctuations is determined by Poissonian statistics with $\delta N_s = N_s^{0.5}$, $\delta N_i = N_i^{0.5}$, $\delta N_p = N_p^{0.5}$ [17]. These fluctuations will result in equal energy fluctuations for the signal and idler $\delta E_s = -\delta E_i$ (and thus reduction of the coherence time) due to the population-dependent blueshift and, hence, equal coherence times in agreement with experiment. The coherence is, thus, a property of the whole OPO system rather than of either the signal or idler separately. The scattering out at the idler is stronger than at the signal due to its higher excitonic content and proximity in energy to uncoupled exciton states. Such scattering affects not only the coher-

ence of the idler state but also that of the signal, which is coupled to the idler and the pump by polariton-polariton pair scattering [11,12].

Taking into account the broadening of the OPO emission due to spontaneous processes discussed above, and the broadening due to fluctuations in polariton number, derived from Eq. (1), the coherence times of the signal and idler are given by

$$1/\tau_{\mathrm{coh}} = 1/(\tau_{\mathrm{sp}} N_s) + \chi^3 \sqrt{\left(\frac{\gamma_i |X_s|^4}{\gamma_i + \gamma_s}\right)^2 N_s + \frac{4|X_p|^4}{(\gamma_i + \gamma_s)^2} (\gamma_i |X_s|^2 - \gamma_s |X_i|^2)^2 N_p}. \quad (2)$$

In the formula, we omit the N_i term from Eq. (1), since $N_i \ll N_s, N_p$, and assume the fluctuations in the signal and idler are independent. Above threshold, the number of polaritons in the pump is almost independent of the excitation power and is given by the threshold value, since with increasing power the additional polaritons are transferred efficiently to the signal and idler [12]. Therefore, the variation of τ_{coh} with occupation is governed mainly by N_s. N_p is estimated to be $\sim 6000 \pm 3000$ at threshold pump powers of ~3–7 mW. We measure the power of the total emission in the signal beam to be $\sim 200\ \mu$W for $P =$ 30 mW. This enables us to deduce the average polariton number in a single signal mode [Fig. 2(a)] to be $\sim 1000 \pm$ 300 at $P = 30$ mW. χ^3 is deduced from the energy shift of the signal of ~0.25 meV at $P = 30$ mW.

Equation (2) was then used to fit the observed variation of τ_{coh} with N_s. The result is shown in Fig. 3(d). At powers close to threshold, N_s is small and the first term in Eq. (1) dominates, resulting in a fast increase of τ_{coh} with I_s as seen experimentally in Fig. 3(c). With increasing N_s, the second term in Eq. (1) increases and eventually dominates, resulting in quasisaturation of τ_{coh} again as in Fig. 3(c) [20]. The overall similarity between the experimental and theoretical variations provides clear evidence for the role of interaction effects in limiting the temporal coherence. The best fit is obtained for $N_s = 2000$ at $P = 30$ mW and $N_p = 3000$, close to the values deduced from experiment. Both the onset of saturation at $N_s \sim 500$ and the maximum value of τ_{coh} of ~450 ps (corresponding to a linewidth of $\sim 2\ \mu$eV) found experimentally are reproduced well, providing further support to the model.

The decrease of the experimental τ_{coh} to 200–300 ps at the highest power of 30 mW may arise from the onset of OPO instabilities [12], when the OPO tends to switch off due to the blueshift: This effect may play an additional role in determining the amplitude of the polariton fluctuations and explain the saturation behavior of the signal intensity in Fig. 2(b) at $P > 20$ mW.

In conclusion, we have shown that polariton-polariton interactions play a dominant role in limiting the temporal coherence of the stimulated emission from microcavity OPOs. The factors limiting the coherence are in marked contrast to those in a noninteracting system such as a laser. Coherence times of individual signal and idler modes have been observed to be similar over the whole excitation range of powers even though the idler is subject to strong additional scattering. This shows that the temporal coherence of stimulated polariton emission is a property of the interacting OPO system rather than of the signal and idler separately. The spatially and spectrally resolved images show that interaction effects coupled with spatial nonuniformity also limit the spatial coherence to distances of order 5–10 μm.

We thank F. P. Laussy and C. Ciuti for helpful discussions. The work was supported by the EU Clermont 2 Project No. MRTN-CT-2003-503677 and EPSRC Grant No. GR/S09838/01.

[1] A. V. Kavokin and G. Malpuech, *Cavity Polaritons* (Elsevier, Amsterdam, 2003).
[2] R. M. Stevenson *et al.*, Phys. Rev. Lett. **85**, 3680 (2000); A. I. Tartakovskii, D. N. Krizhanovskii, and V. D. Kulakovskii, Phys. Rev. B **62**, R13 298 (2000).
[3] P. G. Lagoudakis *et al.*, Phys. Rev. B **65**, 161310(R) (2002).
[4] A. Baas *et al.*, Phys. Rev. B **70**, 161307(R) (2004).
[5] D. N. Krizhanovskii *et al.*, Phys. Rev. B **66**, 165329 (2002).
[6] J. P. Karr *et al.*, Phys. Rev. A **69**, 069901(E) (2004).
[7] S. Savasta *et al.*, Phys. Rev. Lett. **94**, 246401 (2005).
[8] I. Carusotto and C. Ciuti, Phys. Rev. B **72**, 125335 (2005).
[9] G. Messin *et al.*, Phys. Rev. Lett. **87**, 127403 (2001).
[10] We note that, depending on the position of the excitation spot across the sample, a double peak structure of the signal can be observed from a ~5 μm region at powers close to threshold; very similar power dependence to that in Fig. 2(b) is nevertheless seen.
[11] C. Ciuti *et al.*, Phys. Rev. B **63**, 041303(R) (2001).
[12] D. M. Whittaker, Phys. Rev. B **71**, 115301 (2005).
[13] D. Sanvitto *et al.*, Phys. Rev. B **73**, 241308(R) (2006); D. M. Whittaker, Phys. Status Solidi C **2**, 733 (2005).
[14] M. Gurioli *et al.*, Phys. Rev. Lett. **94**, 183901 (2005).
[15] The $g^1(\tau_d)$ function is measured as a function of excitation power at a constant delay τ_d of 200–300 ps. The coherence time is then deduced from $\tau_c = -\tau_d/[(g^1(\tau_d)]$ assuming an exponential decay of $g^1(\tau_d)$.
[16] The idler intensity is too weak to permit study of its coherence close to threshold.
[17] R. Loudon, *The Quantum Theory of Light* (Oxford University, Oxford, 2000).
[18] *VCSEL Design, Fabrication, Characterization and Applications* (Cambridge University Press, Cambridge, England, 1999), p. 240.
[19] D. Porras and C. Tejedor, Phys. Rev. B **67**, 161310(R) (2003).
[20] In the limit of a high signal occupation factor ($N_s >$ 2000), the calculated coherence time slowly decreases due to increase of the second term in Eq. (2).